Nanoscale

Accepted Manuscript

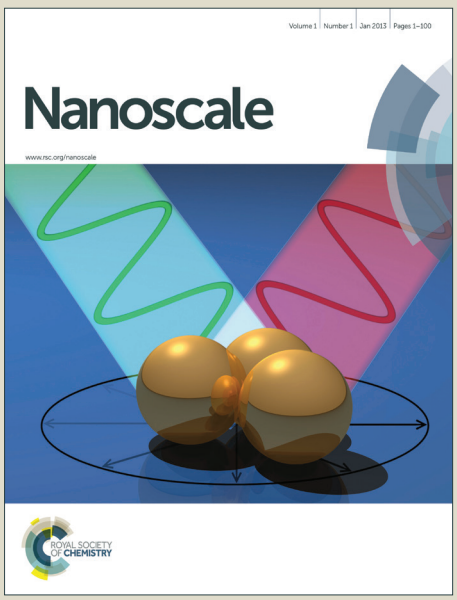

ROYAL SOCIETY OF CHEMISTRY

www.rsc.org/nanoscale

Nanoscale

ARTICLE

Received 00th January 20xx,
Accepted 00th January 20xx
DOI: 10.1039/x0xx00000x

a. www.rsc.org/

Smart Magnetic Nanoplatform for Synergistic Anticancer Therapy by Maneuvering the Mussel-inspired Functional Magnetic Nanoparticles for pH Responsive Anticancer Drug Delivery and Hyperthermia

Arathyram Ramachandra Kurup Sasikala[1‡], Amin GhavamiNejad[1‡], Afeesh Rajan Unnithan[1, 2*], Reju George Thomas[3], Myeongju Moon[4], Yong Yeon Jeong[3], Chan Hee Park[2*] and Cheol Sang Kim [1, 2*]

We report the versatile design of a smart nanoplatform for thermo-chemotherapy treatment of cancer. For the first ti... in literature, our design takes advantage of the outstanding properties of mussel-inspired multiple catecholic groups presenting unique copolymer poly (2-Hydroxyethyl methacrylate-co-dopamine methacrylamide) p(HEMA-co-DMA), to surface functionalize the superparamagnetic iron oxide nanoparticles as well as to conjugate borate containing anticancer drug Bortezomib (BTZ) in a pH-dependent manner for the synergistic anticancer treatment. The unique multiple anchoring groups can be used to substantially improve the affinity of the ligands to the surfaces of the nanoparticles to form ultrastable iron oxide nanoparticles with control over their hydrodynamic diameter and interfacial chemistry. Thus the BTZ–incorporated-bio-inspired-smart magnetic nanoplatform will act as hyperthermic agent that delivers heat when an alternating magnetic field is applied while the BTZ-bound catechol moieties act as chemotherapeutic agents in cancer environment by providing pH-dependent drug release for the synergistic thermo-chemotherapy application. The anticancer efficacy of these bio inspired multifunctional smart magnetic nanoparticles were tested both in vitro and in vivo and found that these unique magnetic nanoplatform can be established to endow for the next generation of nanomedicine for efficient and safe cancer therapy.

1. Introduction

Cancers are among the leading causes of death worldwide, accounting for millions of deaths every year[1]. The high complexity and wide variations in different types of cancer have made it impossible to find an optimal and generally applicable treatment.[2] However, recent advancements in nanomedicine have made it possible to provide treatment modalities that are more effective against cancer. [1] Among these, magnetic nanoparticles (MNPs) have gained significant attention for the theranostic application of cancer due to their excellent biocompatibility and unique magnetic properties, such as superparamagnetism. [3-5] Magnetic nanoparticle-mediated hyperthermia has emerged as a promising modality for cancer treatment due to the unique heat-generating properties of super paramagnetic iron oxide nanoparticles (SPIONs) under an alternating magnetic field (AMF). [6, 7] During hyperthermia, the body tissue temperature increases to around 40 to 45 °C by delivering heat obtained from external sources to destroy cancerous cells or to prevent their further growth.[8] Several studies have revealed that hyperthermia acts synergistically with radiotherapy or chemotherapy, providing a promising strategy to improve cancer therapy. [9-11]

The ultimate goal of a nanoparticle-mediated strategy to treat cancer involves controlled, targeted delivery of therapeutics to tumor sites. [12-14] Doing so improves the specificity and efficiency of cancer treatment while minimizing side effects. In order to achieve controlled, targeted delivery, nanoparticles should be properly functionalized with different functional moieties, such as targeting ligands[15] and stimuli responsive polymers susceptible to various stimuli.[16, 17] To this end, stimuli-responsive polymer-functionalized superparamagnetic Fe_3O_4 nanoparticles incorporating chemotherapeutics are ideal candidates to deliver thermo-chemotherapy.

Recently, mussel-inspired dopamine-containing polymers have been extensively implemented for a variety of practical applications due to their remarkable chemical properties. [18, 19] Recently our group also reported a mussel inspired smart magnetic nanofibers for hyperthermic chemotherapy. [20] Dopamine is a versatile candidate for bioapplications since it has excellent biocompatibility and low cytotoxicity.[21-23] The catechol groups in dopamine exhibit a strong binding affinity towards a variety of metal oxides via irreversible metal-ligand exchange or reversible metal-ligand complexation and

[1]Department of Bionanosystem Engineering, Graduate School, Chonbuk National University, Jeonju 561-756, Republic of Korea.
[2]Mechanical Design Engineering, Chonbuk National University, Jeonju 561-756, Republic of Korea.
[3]Department of Radiology, Chonnam National University Hwasun Hospital, Chonnam National University Medical School, Gwangju 501-746, Republic of Korea
[4]DKC corporation (BioActs), Incheon, South Korea
‡These authors contributed equally.

bonding.[24] Several studies have reported that dopamine analogues and polymer-catechol conjugates are desirable for surface functionalization of SPIONs.[25, 26] Many of these studies have used mono-functional groups to stabilize the iron oxide nanoparticles. However, these ligands exhibit a weak binding affinity towards the surface of the nanoparticles, and these can be easily displaced by biomolecules bearing amine and carboxylic functional groups.[27] Therefore, multiple anchoring groups can be used to substantially improve the affinity of the ligands to the surfaces of the nanoparticles. Furthermore, this will lead to the formation of ultrastable iron oxide nanoparticles with control over their hydrodynamic diameter and interfacial chemistry.[28]

In recent decades, a myriad of stimulus-responsive nanosystems have received much attention for use as efficient drug delivery platforms to improve therapeutic applications.[29] Among the different stimuli that are possible, pH-responsiveness has been the most extensively investigated for delivery of anticancer drugs since tumors have a slightly acidic extracellular environment, which allows for pH-triggered release of the anticancer drugs.[30-32] Previous studies have demonstrated that in addition to the strong binding ability of the catechol groups for metal oxides, the catechol groups can also be utilized to bind and release borate-containing anticancer drugs, such as BTZ, in a pH-dependent manner.[33, 34] An important characteristic of the boronic acid catechol conjugate is the formation of dynamic covalent chemistry between catechol and BTZ, reversibly bonding in a pH-sensitive manner.[34]

Here, we report on the design and development of novel mussel-inspired polymer-coated SPIONs incorporating the anticancer drug BTZ to deliver a combination of both hyperthermia and chemotherapy. We have applied a slightly different approach to introduce multiple catecholic groups along the polymeric chains by using a biocompatible copolymer poly (2-Hydroxyethyl methacrylate-co-dopamine methacrylamide) p(HEMA-co-DMA) (abbreviated as HEDO) synthesized via radical polymerization to easily accommodates several anchoring groups that can bind with metal nanoparticles as well as the borate-containing anticancer drug BTZ. Thus the prepared drug-loaded magnetic nanoparticles will act as the hyperthermic agents by delivering heat when an alternating magnetic field is applied and as chemotherapeutic agents by releasing the borate-containing anticancer drug BTZ bound to the catechol moieties in a pH-dependent manner.

2. Experimental Section

2.1. Materials: Iron(III) acetylacetonate [$Fe(acac)_3$], 1,2-hexadecanediol (90%), oleic acid, oleylamine (70%), benzyl ether (98%), methacryloyl chloride, sodium borate (99.5%), sodium bicarbonate(99%), 3,4-dihydroxyphenethylamine hydrochloride, 2-Hydroxyethyl methacrylate, azobisisobutyronitrile, tetrahydrofuran (THF), dimethylformamide (DMF), dimethyl sulfoxide (DMSO) ethanol , hexane, diethyl ether, methylene chloride were purchased from Sigma Aldrich, South Korea.

2.2. Synthesis of Iron oxide nanoparticles (IONPs) Monodisperse iron oxide nanoparticles were synthesized by carrying out the high-temperature reduction/decomposition of metal acetylacetonate[35] with some modifications. The amount of surfactants and solvent used in the reaction were adjusted to control the size of the particles produced during one-step reduction/decomposition. In a typical experiment, a one pot reaction was carried out with metal precursor Fe(acac)3(2 mmol), 1,2-hexadecanediol (10 mmol), surfactants [oleic acid (6 mmol) and oleylamine (6 mmol)], and solvent [benzyl ether (10 ml)] under a nitrogen flow. The mixture was heated to 200 °C for 2 h with nitrogen gas flow protection, and the mixture was then further heated to 300 °C for 1h. The mixture black in color was obtained and was allowed to cool down to room temperature. The MNPs were precipitated by adding ethanol and were separated via centrifugation. The black product was again dispersed in hexane with oleic acid (~0.05 mL) and oleylamine (~0.05 mL). Centrifugation (4000 rpm, 20 min) was applied to remove the undispersed residue, and the product was precipitated with ethanol. This washing procedure was repeated at least 3 times, and the as obtained MNPs were dried at 40 °C in a vacuum and were stored in a sealed glass vial at 4^0C.

2.3. Synthesis of dopamine methacrylamide (DMA) Dopamine methacrylamide (DMA) was prepared and characterized according to a modified method derived from a previously reported strategy.[36] A gray powder with a yield of 85% was obtained as the product, and the structure of the monomer was confirmed via ^{1}H-NMR. Deuterated dimethyl sulfoxide (d-DMSO) was used as a good solvent for the pure monomer. ^{1}H-NMR (400 MHz, DMSO, 273 K), 6.4–6.6(3H, m, Ph), 5.5 (1H, d, CH2=C), 5.25 (1H, d, CH=C–), 3.3 (2H, q, CH2-NH-), 2.5 (2H, tr, CH2-Ph), 1.8 (3H, s, CH2 C–).

2.4. Synthesis and Characterization of p(HEMA-co-DMA), abbreviated as HEDO: 42 mmol of 2-Hydroxyethyl methacrylate and 8.4 mmol of DMA monomers were added to a 50 mL round bottom flask containing 30 mL of DMF under nitrogen gas. After 20 min of nitrogen bubbling, 120 mg of azobisisobutyronitrile was added to the flask, and the solution was heated up to 70 °C and stirred overnight. Next, the solution was added drop wise to 400 mL of diethyl ether while stirring to precipitate the synthesized copolymer. The purified copolymer was dried overnight in a vacuum oven at room temperature. A white solid was obtained with a yield of 62%. The synthesized samples were analyzed using ^{1}H-NMR spectroscopy, and the results are illustrated in Figure S1 of the Supporting Information. The copolymer consisted of relatively short chains with a molecular weight of about 2800 Da.

2.5. Synthesis of Iron oxide nanoparticles functionalized with HEDO, abbreviated as HEDO-Fe_3O_4: The as-obtained oleic acid-stabilized nanoparticles were re-dispersed into dimethylformamide (DMF) to form the dispersion at a concentration of 1 mg particles/ml of solvent. In the next step a 20 wt.% copolymer solution (in DMF) was added drop v

into the nanoparticle suspension (1: 2 v/v) under constant mechanical stirring at 500 rpm in order to initiate the ligand exchange between the oleic acid and the catechol groups. This suspension was kept at room temperature for 24 h under constant mechanical stirring. Excessive dispersants were removed by washing the suspension several times with double-distilled water in order to obtain the bio inspired HEDO-Fe_3O_4 nanoparticles.

2.6. Preparation of the HEDO-Fe_3O_4- BTZ nanoparticles: The HEDO-Fe_3O_4-BTZ nanoparticles were prepared by using the following procedure. A fixed amount of BTZ (2 mM) was added to a 20 wt.% solution of HEDO in dimethylformamide, and the solution was kept overnight in a shaking incubator at room temperature to initiate complexation between the catechol functionalities and the boronic acid active site of BTZ. A known concentration of oleic acid-stabilized Fe_3O_4 nanoparticles in 1 ml DMF was added into the obtained HEDO-BTZ suspension while applying constant mechanical stirring at 500 rpm in order to initiate ligand exchange between the oleic acid and the unreacted catechol groups. This suspension was kept at room temperature for 24 h under constant mechanical stirring, and in the next step, the precipitate was magnetically separated, washed with pH 7.4 water and subsequently stored at 4 °C until further use. The drug concentration in the supernatant was measured by capturing the UV spectra of BTZ with a previously-obtained calibration curve with a dilution series. The amount of drug incorporated into HEDO-Fe_3O_4 was estimated at 60% through the following equation.[37]

$$\%\ \text{Entrapment efficiency} = \frac{\text{Initial concentration of drug} - \text{Drug content in the supernatant}}{\text{Initialconcentration of drug}} \times 100$$

The possibility of complexation between boron and catechol groups in an aprotic solvent has been previously studied in other works,[38, 39]and the availability of catechol moieties for further surface functionalization of the SPIONs was evaluated using UV-VIS photospectroscopy, as shown in Figure S4 of the supporting information.

2.7. Characterization of the nanoparticles: The H-NMR spectra were recorded in dimethyl sulfoxide (DMSO) with a Bruker AM 400 spectrometer (400 MHz). The molecular weight (Mw) and molecular weight distribution (Mw/Mn) of the copolymer samples were determined by using a size exclusion chromatography (SEC) system equipped with a refractive index detector (PL-GPC110, Polymer laboratories). X-Ray powder diffraction analysis was carried out on a Rigaku X-ray diffractometer (Cu Ka, k= 1.54059 Å) over Bragg angles ranging from 20° to 80°. The size, morphology and crystallography of the as synthesized Fe_3O_4 nanoparticles as well as the HEDO-Fe_3O_4 nanoparticles was investigated via transmission electron microscopy (TEM, JEOL JEM, Japan), and the corresponding SAED (specific area electron diffraction) pattern was also studied. The size distributions of the nanoparticles were also confirmed by using a DLS instrument (Brookhaven Instruments Corporation). The bonding configurations of the samples were characterized by means of their FTIR spectra using a Paragon 1000 Spectrometer (Perk Elmer). The elemental composition and the surface state of the samples were checked via X-ray photoelectron spectroscopy (XPS, AXIS-NOVA, Kratos, Inc.) with an Al Kα irradiation source, and the magnetic characterization was carried out on a physical property measurement system (PPMS, model 6000).

2.8. In vitro Hyperthermia studies of HEDO-Fe_3O_4 and SAR measurement: The alternating magnetic field (AMF) induced heating in HEDO-Fe_3O_4, and this behavior was studied by measuring the time-dependent rise in temperature of the samples when an AMF generated from an alternating magnetic field generator (OSH-120-B, OSUNG HITECH, Republic of Korea) was applied at room temperature. Different concentrations of HEDO-Fe_3O_4 (0.5, 1, 2 and 3 mg) were dispersed in 1 ml of MilliQ water in an Eppendorf tube, which was then placed at the center of a water-cooled induction coil made of copper with an inner diameter of 60 mm (three turns). The strength and frequency of the magnetic field were adjusted to 12.57 kA/m and 293 kHz, respectively. The samples were heated for 600 s, and the heating characteristics were automatically recorded using type-T thermocouples and a real-time data acquisition system (NI DAQ^R, National instrument, USA) with the Lab VIEW program. Before each experiment, the temperature was calibrated and stabilized for 10 min. The heating efficiency of the samples was quantified by calculating the specific absorption rate (SAR), following the procedure that was described earlier.[40] The SAR values were calculated using the equation

$$SAR = C\left(\frac{\Delta T}{\Delta t}\right)\frac{1}{m_{magn}}$$

where C is the sample-specific heat capacity calculated as the mass-weighted mean value of magnetite and water. The heat capacity of magnetite is not considered in the current study, since it is present at a low concentration, and hence the heat capacity for water (4.186 J $g^{-1}K^{-1}$) is considered as the heat capacity of the sample. [41] $\Delta T/\Delta t$ is the initial slope of the time-dependent temperature curve, which is initially obtained for 60 s once after the magnetic field is switched on since the curve follows a linear relationship in this regime. The value of m_{magn} is considered as the amount of magnetite per total amount of magnetite and water.

2.9. Kinetics of the pH-dependent drug release: The pH-dependent drug release from HEDO-Fe_3O_4-BTZ is analyzed by performing a procedure that is quite similar to that used to measure 0drug entrapment efficiency. In a typical procedure, a predetermined suspension of drug-loaded nanoparticles was made in Phosphate-buffered saline (PBS) buffer at different pH levels, including physiological (pH 7.4) and acidic (pH 5) conditions, and these samples were placed in a shaking incubator at 37 °C. At different time intervals, 1 ml of the release solution (PBS) were taken out and replaced with 1 ml of fresh PBS in order to maintain a constant volume. The

amount of BTZ that was released was quantified by capturing the UV–visible absorption spectra (HP 8453 UV–vis spectroscopy system, Germany) at a wavelength of 270 nm. Triplicate samples were used to ensure accuracy.

2.10. In vitro cell culture studies: Murine fibroblast (NIH3T3), murine squamous carcinoma (SCC7), and murine colon carcinoma (CT-26) cell lines were purchased from ATCC® (Manassas, VA USA).

2.10.1. Biocompatibility study of HEDO-Fe_3O_4: The biocompatibility of HEDO-Fe_3O_4 against NIH3T3 cells was evaluated by using an MTS assay. The cells were seeded into a 96-well plate at a density of 10^4 cells /well. The cells were cultured for one day in an incubator with a humidified CO_2 atmosphere at 37 °C. HEDO-Fe_3O_4 was added to the cells in triplicate in order to analyze the cytocompatibility for different concentrations of HEDO-Fe_3O_4, ranging from 0.01 µg/ml to 100 µg/ml. The cells were incubated for 24 hours after treatment, and then 20 µl of MTS reagent were added to each of the treated wells and were incubated for 4 hours. Finally, the absorbance at 490 nm was measured using a microplate reader.

2.10.2. Intracellular localization study of HEDO-Fe_3O_4: The intracellular localization of the nanoparticles is very important in order to effectively deliver the cancer therapy. Therefore, the intracellular uptake of the HEDO-Fe_3O_4 nanoparticles was investigated via Prussian blue staining in CT-26 and SCC7 to qualitatively verify the specific uptake in the cancer cells. CT-26 and SCC7 cells (5 x 10^5 cells/well) were seeded in an 8-well chamber slide (Lab-Tek2, Utah,USA) supplemented with DMEM and RPMI medium (Thermo Scientific, Utah, USA), respectively. Both contained 10% FBS and 1% penicillin–streptomycin, and the cells were kept at 37 °C overnight in a humidified 5% CO_2 atmosphere. After 24 hours, both cell samples were washed twice with PBS to remove the medium. In order to study the intracellular localization of the nanoparticles on both cell lines, 25 µg/ml of HEDO-Fe_3O_4 were added and incubated for another 2 hours. The cells were fixed with 4% PFA for 15 min, and each well was supplemented with 100 µl of 4% potassium ferrocyanide (II) trihydrate and 4% HCl solution (in PBS) and was then incubated for an additional 20 minutes. The cells were counter-stained with a nuclear fast red stain, and the images were collected with an inverted light microscope.

2.10.3. In vitro hyperthermia study using HEDO-Fe_3O_4-BTZ: The synergistic effects of HEDO-Fe_3O_4-BTZ were evaluated on SCC7 cell lines in the absence and presence of an AMF. The cytotoxicity of the HEDO-Fe_3O_4-BTZ nanoparticles was determined by conducting an MTS assay. SCC7 cancer cells were seeded at a density of 5×10^4 cells into 24 well plates and were cultured in DMEM medium in an incubator with a humidified 5% CO_2 atmosphere at 37 °C. After 24 h of incubation, 1 mg/ml of HEDO-Fe_3O_4-BTZ was added to the cells, and the samples were incubated for 6 more hours with an additional set of blank cells kept as controls. HEDO-Fe_3O_4-BTZ was administered into SCC7 cells to assess the improvement in therapeutic efficacy resulting from combined hyperthermia and chemotherapy. The samples were divided into treated (AMF on), untreated (AMF off), and control groups. One set (in triplicate) of plates containing the treated adherent cells was exposed to AMF for 10 min (12.57 Oe, 2[illegible] kHz) in a sterile environment while the untreated sample (i[illegible] triplicate) was isolated into a mini petri dish for the sam[illegible] period of time to cancel out the environmental effect on cell death. After the hyperthermia treatment on all samples, fres[illegible] RPMI media was added and incubated in a 24-well plate again for 30 minutes in an incubator with a humidified 5% CO[illegible] environment at 37 °. After 1 day, 50 µl of MTS reagent (Promega, USA) were added to each of the wells, and the plat[illegible] was incubated for an additional 4 hours. The absorbance at 490 nm was then measured using a microplate reader. The procedure was repeated for day 3 & 5.

2.10.4. Live/dead assay: A qualitative analysis of the in vitro hyperthermia was conducted by performing a live/dead cell cytotoxicity assay (Molecular Probes, USA). SCC7 cells were seeded at a density of 5×10^4 cells in a 24-well plate with a coverslip and were cultured in RPMI medium in an incubator with a humidified 5% CO_2 environment at 37 °C. After one day of incubation, 1 mg/ml of HEDO-Fe3O4-BTZ was added, and the samples were incubated for an additional 6 hours. The treated coverslip was isolated, washed three times with warm PBS, and subjected to hyperthermia for 5 minutes after optimizing the hyperthermia temperature. The untreated coverslip was kept separately in a mini petri dish in an incubator with a humidified 5% CO_2 environment at 37 °C in order to rule out environmental effect on cell death for the duratino of the hyperthermia treatment. 1 day after the hyperthermia had been administered, the HEMA-DOPA sample was treated with 200 µl of calcein AM (4 µM) and ethidium homodimer (0.5 µM) dissolved in PBS for 30 minutes at room temperature. The coverslip containing the cells was viewed directly under a fluorescent microscope at a standard fluorescein band pass filter for calcein and Texas Red ™ dye filter for ethidium homodimer. The apoptosis-inducing effect of HEDO-Fe_3O_4 and HEDO-Fe_3O_4-BTZ was qualitatively evaluated by using a Magic Red caspase detection kit that uses a red fluorogenic substrate for caspases 3 and 7. The treated cells (24 h post hyperthermia), were further incubated with Magic Red caspase detection kit for 45 mins.

2.11. In vivo tumor inhibition study using HEDO-Fe_3O_4-BTZ: The anticancer efficacy of HEDO-Fe_3O_4-BTZ induced by the thermo-chemotherapy was further tested in vivo. In vivo experiments were performed in accordance with the guidelines of the Ethics Committee of the Chonnam National University Medical School (CNU IACUC-H-2011-5). Athymic mice (nu/nu-ncr, Balb/c mice, 5–6 weeks old, 20–25 g) were obtained from Jungang Lab Animal, Inc., Korea. In a typical procedure, the mice were subcutaneously injected with SCC7 cancer cells ($1x10^6$ cells), and we waited until the tumor size grew to 100 mm^3. The mice were randomly allocated into three experimental groups of 3 rats each (n=3). The first group was used as control, i.e., without any treatment. The second and third groups were injected with HEDO-Fe_3O_4-BTZ in PBS solution (40 mg/kg) via an intra-tumour route, and they were divided into treated (AMF on) and untreated groups (AMF off)

The anticancer efficacy was analyzed by administering hyperthermia to the mice in the treated group by placing the mouse in the middle of a water-cooled magnetic induction coil and applying an AC magnetic field (293 kHz at 12.57 kA/m) for 10 minutes after reaching the hyperthermia temperature at the tumour. The hyperthermia treatment was repeated twice by following the same procedure with a three-day interval between each treatment. After three cycles of hyperthermia, the tumour degradation was evaluated by measuring the tumour weight and tumour volume of the groups. The tumour volume was measured using a digital Vernier caliper (Mitutoyo Corp., Kawasaki, Japan) and was calculated by using the following equation[42]

$$Volume = length \times width^2 / 2.$$

The tumor was then excised and weighed (Kent Scientific, Connecticut USA), and the weight (grams) was plotted against the control.

3. Results and Discussion

Monodisperse iron oxide nanoparticles (IONPs) were synthesized by the thermal decomposition method as described earlier[35]. Synthesis of biocompatible multiple catecholic groups presenting copolymer p(HEMA-co-DMA), abbreviated as HEDO has been carried out by radical polymerization and the characterization were performed (Figure S1 of the Supporting Information). The as prepared mussel inspired copolymer has been utilized for the surface functionalization of the IONPs by immobilizing the catechol moieties present in the polymer onto the surface of the Fe_3O_4 nanoparticles through the metal ligand exchange to form a thin layer of coating. Thus the resulting bio inspired magnetic nanoparticles are abbreviated from here onwards as HEDO-Fe_3O_4.

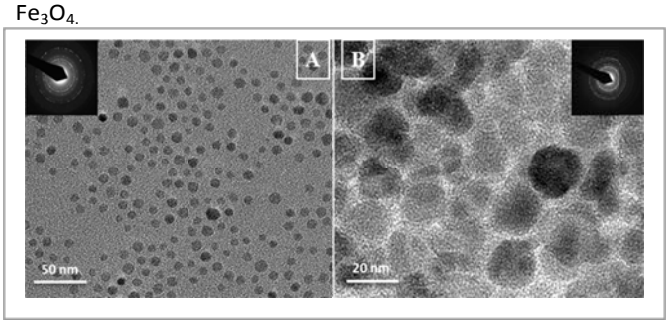

Figure 1. TEM images of (A) Fe_3O_4 (inset SAED) and (B) HEDO-Fe_3O_4 (inset SAED)

The crystal structures of the Fe_3O_4 and HEDO-Fe_3O_4 were analyzed using powder X-ray diffraction XRD patterns (Figure S2 of the Supporting Information) and found that the diffraction peaks appeared were in good agreement with the characteristic peaks of standard magnetite crystal. The size and shape of the Fe_3O_4 and HEDO-Fe_3O_4 nanoparticles were inspected via transmission electron microscopy (Figure 1), and both nanoparticles were observed to possess uniform distribution with a spherical morphology. The size of the Fe_3O_4 nanoparticles were found to be less than 15 nm, and the polymer coated HEDO-Fe_3O_4 nanoparticles exhibited a very small increase in their diameter of around 3–5 nm. The DLS results also verified these observations (Figure S3 of Supporting Information). This is due to the thin layer of polymer coating formed as a result of the immobilization of the catechol moieties present in the polymer onto the surface of the Fe_3O_4 nanoparticles through metal ligand exchange.

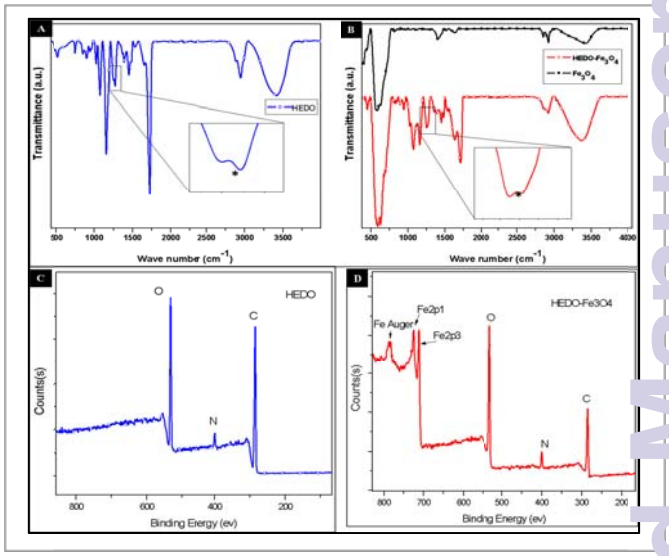

Figure 2. FTIR spectra of A) HEDO and B) Fe_3O_4 & HEDO-Fe_3O_4 and XPS of C) HEDO & D) HEDO-Fe_3O_4

FTIR was performed in the spectral range between 500 and 4000 cm^{-1} for HEDO, Fe_3O_4 and HEDO-Fe_3O_4 in order to analyze the bonding between HEDO and Fe_3O_4 nanoparticles (Figure 2A & B). The FTIR spectrum of HEDO-Fe_3O_4 is nearly identical to that of pure HEDO. However, in comparison to the FTIR spectrum of HEDO, a strong absorption band can be identified at 580 cm^{-1}, and this band is assigned to the vibrations of the Fe–O group. The existence of the bonding between Fe_3O_4 nanoparticles and polymeric chains was confirmed, and in addition, the IR spectrum for HEDO-Fe_3O_4 shows that phenolic C–O–H stretching vibrations (1290 cm^{-1}) of the catechol groups in HEDO significantly decrease after ligand exchange with Fe_3O_4, indicating an oxidation of the catechol moiety to a quinone structure.

The XPS spectrum of the HEDO-Fe_3O_4 nanoparticles was compared to that of pure HEDO (Figure 2C&D). The surface chemical composition of HEDO-Fe_3O_4 was confirmed via XPS measurements, and as expected, the XPS data for HEDO only exhibited C1s (284.7 eV), O1s (531 eV), and N1s (399 eV) peaks while the Fe_3O_4-binding on HEDO can be seen from the binding energy peaks of Fe2p3/2 and Fe2p1/2 at 711.1 eV and 724.6 eV, respectively, which is in agreement with the reference values for Fe_3O_4.[43] XPS is a surface-sensitive technique since it probes the outermost 5–10 nm of the sample.[44] Therefore, an XPS analysis also confirmed the presence of a thin HEDO layer coated onto the Fe_3O_4.

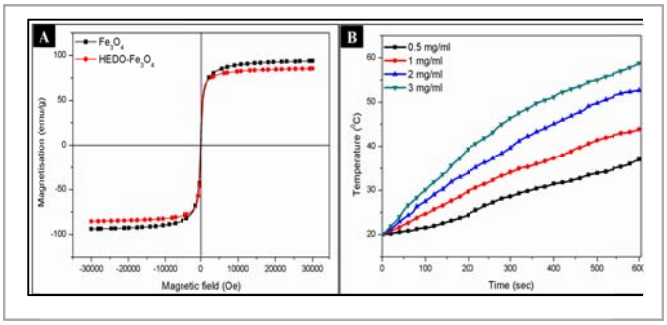

Figure 3. (A) Field-dependent magnetization of Fe_3O_4 and HEDO-Fe_3O_4, (B) AMF-induced heating ability of HEDO-Fe_3O_4 at different concentrations.

The magnetic properties of Fe_3O_4 and HEDO-Fe_3O_4 were investigated by measuring magnetization as a function of the applied field at 300K (Figure 3A). Both types of nanoparticles were found to exhibit superparamagnetic behavior with no coercivity or remanence. Fe_3O_4 and HEDO-Fe_3O_4 were also observed to display high saturation magnetization values with magnetization values of 93.87emu/g and 85.3emu/g, respectively. These high magnetization values are extremely useful in administering magnetic hyperthermia as well as in enabling targeting applications since the particles respond rapidly to an external magnetic field.[45] The magnetic field dependent heating ability of HEDO-Fe_3O_4 was measured at various concentrations (Figure 3B) and found that 1 mg/ml of HEDO- Fe_3O_4 reached a hyperthermic temperature of ~43 °C within 600 s. The heating ability of 1 mg/ml HEDO- Fe_3O_4 were quantified by measuring the specific absorption rate (SAR) from the time dependent heating curves, since the concentration is optimized to use for hyperthermia application. The SAR value obtained to be 181.31 W/g.

In order to prepare the smart Magnetic Nanoplatform for pH responsive anticancer drug release and hyperthermia, the borate-containing anticancer drug has been bound to the magnetic nanoparticle. The drug bound magnetic nanoparticles (HEDO-Fe_3O_4-BTZ) are prepared by the initial mixing of the anticancer drug with HEDO to initiate the complexation between catechol functionalities and boronic acid active site of BTZ followed by adding IONPs to initiate the ligand exchange between the oleic acid and the unreacted catechol groups in the HEDO-BTZ suspension. The availability of catechol moieties for further surface functionalization of the SPIONs after mixing HEDO with BTZ was evaluated using UV-VIS photospectroscopy (Figure S4 of the supporting information).

The pH-sensitive binding of BTZ onto HEDO-Fe_3O_4 nanoparticles (HEDO-Fe_3O_4-BTZ) was confirmed by observing the release of BTZ in buffer solutions at different pH levels to mimic the tumor environment (pH=5.0) and normal tissue or blood (pH=7.4). As illustrated in Figure 4, the release of BTZ from the HEDO-Fe_3O_4-BTZ nanoparticles was pH dependent. During a 12 h period, ~20% of the BTZ was released from the HEDO-Fe_3O_4-BTZ nanoparticles that were kept at a pH of 7.4 while 86% of the BTZ was observed to be released at a pH of 5. These results clearly indicate the pH-dependent drug release of HEDO-Fe_3O_4-BTZ nanoparticles. This behavior is a result of the pH-dependent BTZ dissociation from the catechol-presenting HEDO-Fe_3O_4-BTZ nanoparticles. The complexation between BTZ and the catechol groups present in the HEDO-Fe_3O_4 dissociate at a low pH, which contributes to the smart drug release, while at physiological pH or higher, the HEDO-Fe_3O_4-BTZ nanoparticles are inactive, resulting in a minimum drug release. Therefore, this smart chemotherapeutic platform can be considered to be unique in such a way that it is inactive in normal tissue but allows BTZ activity to be triggered in cancerous tissue, where the pH is low. This behavior has the potential to reduce the side effects caused by the early release of chemotherapeutic agents during circulation, thus improving specific drug delivery.

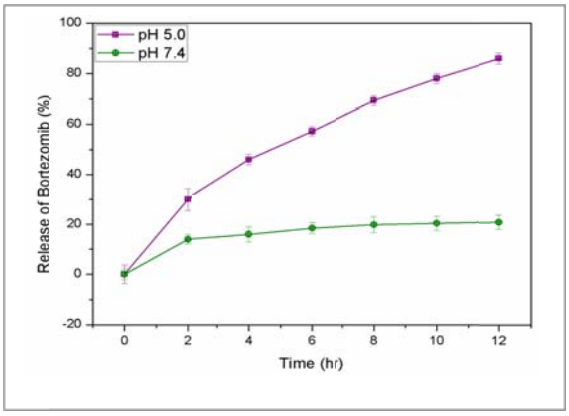

Figure 4. BTZ release from HEDO-Fe_3O_4 –BTZ nanoparticles over time in buffers at two different pH values pH 5.0, and 7.4

Biocompatibility is an important factor to consider before a material is used in any biological application. Fe_3O_4 nanoparticles are well known to be promising candidates for use in biomedical applications because they possess excellent biocompatibility and stability in a physiological environment.[46] We used an MTS assay to investigate the biocompatibility of different concentrations of HEDO-Fe_3O_4 in murine fibroblast (NIH3T3) cell lines after 1-day, 3 day and 5 day period of incubation. The cell viability for HEDO-Fe_3O_4 was almost equal to that of control for all concentration ranges from 0.01 mg/ml to 5 mg/ml, even after 5 days of incubation (Figure 5), which confirmed its excellent biocompatibility.

The cellular uptake of HEDO-Fe_3O_4 nanoparticles was observed via Prussian blue staining, as shown in Figure 5 B&C. Prussian blue staining is an efficient method to qualitatively analyze the uptake of iron oxide nanoparticles that are stained blue. Here we observed that, murine squamous carcinoma (SCC7), and murine colon carcinoma (CT-26) cell lines exhibited an increased uptake of HEDO-Fe_3O_4 nanoparticles after a short incubation time of 2 hours. Moreover the intracellular uptake of HEDO-Fe_3O_4 nanoparticles was almost the same in both cell lines, which indicate that no specific uptake mechanism is involved for the uptake of HEDO-Fe_3O_4 and both cancer cell lines had an equal chance to uptake the nanoparticles. This can be explained by the small size of the nanoparticles. Thus the improved uptake without specificity towards a specific cancer cells makes HEDO-Fe_3O_4 q

suitable for use in clinical application in a wide range of cancer types.

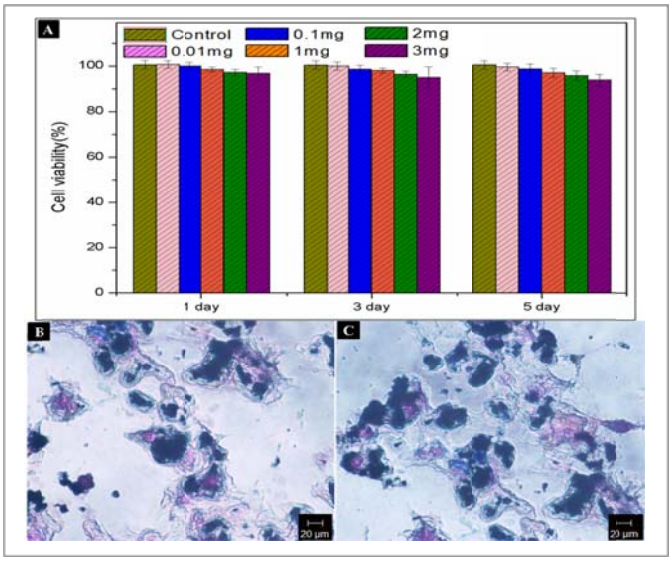

Figure 5. A) In vitro biocompatibility of HEDO-Fe_3O_4 taken at different concentrations, B&C) Intracellular localization of HEDO-Fe_3O_4 by Prussian blue staining in B) CT-26 (murine colon cancer) and C) SCC7 (murine head and neck cancer).

After the biocompatibility and intra cellular uptake of HEDO-Fe_3O_4 nanoparticles was confirmed, the applicability of the mussel inspired magnetic nanoparticles for generating the localized anticancer effects in response to an AMF was investigated. The anticancer efficacies were tested on SCC7 cell lines and compared in three scenarios, which include hyperthermia alone (HEDO-Fe_3O_4, AMF on), drug alone (HEDO-Fe_3O_4-BTZ, no AMF) and combined hyperthermia and chemotherapy (HEDO-Fe_3O_4-BTZ, AMF on) and the cell viabilities were tested at 24 hour after hyperthermia application (Figure. 6).

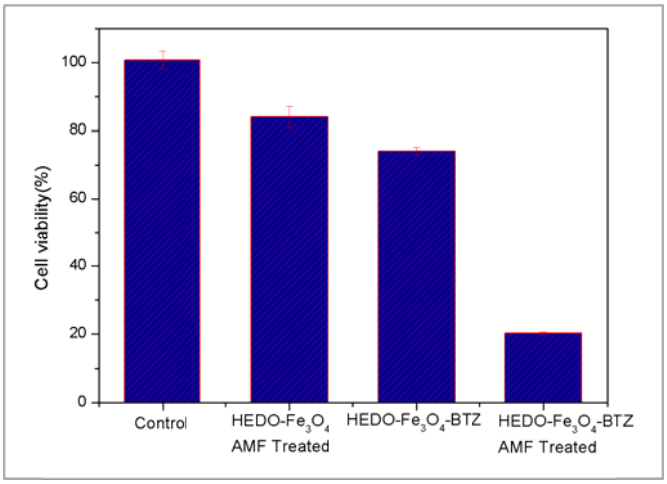

Figure 6. A) In-vitro anticancer effects of HEDO-Fe_3O_4-BTZ on SCC7 cell lines.

It was found that the average viabilities of the treated cells are decreased considerably after the treatments. In hyperthermia alone group, accounted for the death of a significant amou of cells (16 %) even after a 10 minute of AMF exposure whereas the chemotherapy alone group accounted a 26% c cell death due to the cancer cell specific BTZ release after 2 hour of incubation compared to the control sample. A expected, cell death due to the combination of hyperthermia and chemotherapy was found to be 80% due to the synergist effect of both hyperthermia and chemotherapy. Compared to the hyperthermia alone group and chemotherapy alon group, the combination therapy group exhibited an enhanced anticancer efficacy. This may be due to the physiological effect of mild hyperthermia, which facilitate the HEDO-Fe_3O_4-BTZ extravasation in cancer cells, which bring about the enhance drug accumulation along with effective hyperthermia [47]. Thes results prove the enhanced anticancer efficacy of HEDO-Fe_3O BTZ, in combination with hyperthermia.

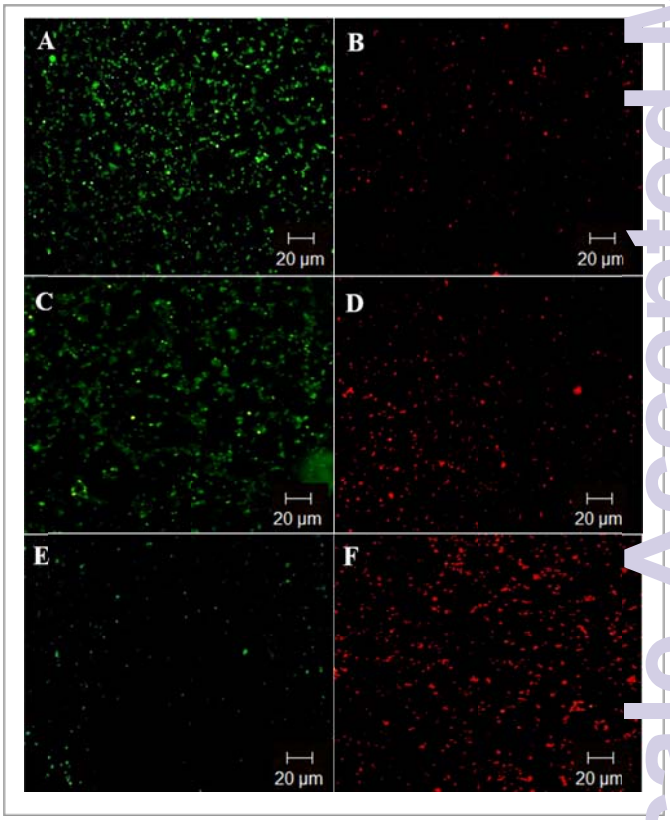

Figure 7. A-F) Live/dead assay displaying the localize anticancer effect. A-E) cells stained with calcein and B-F) cells stained with ethidium homodimer. A&B) Hyperthermia alon sample (HEDO-Fe_3O_4, AMF on), C&D) Chemotherapy alone sample (HEDO-Fe_3O_4-BTZ), A&D) sample, E&F) combinatio therapy sample (HEDO-Fe_3O_4-BTZ, AMF on).

The anticancer effects of the combined scenario in comparison to hyperthermia alone and chemotherapy alone were further confirmed by performing a live/dead cell cytotoxicity assay, as shown in Figure 7. The cell viability was assessed using calcein AM staining, and found that the hyperthermia alone or chemotherapy alone samples were found to have minor effects in terms of their cell viability relative to the combined scenario, as evidenced by the green fluorescence. This was further examined by a dead assay using an ethidium homodimer. For the dead assay, the red fluorescence intensity of the combination therapy applied samples was higher than that of the other samples, indicating greater ethidium homodimer uptake through the damaged cell membrane and nucleic acid attachment. The results are in good agreement with the results of the in vitro study. Cell death in chemotherapy alone can be accounted by the drug cytotoxicity while the enhanced cell death in the combined hyperthermia and chemotherapy applied samples can be the result of the synergistic effect of hyperthermia along with the drug release. This further confirmed the therapeutic efficacy of HEDO-Fe_3O_4-BTZ to be applied for the combination therapy for cancer.

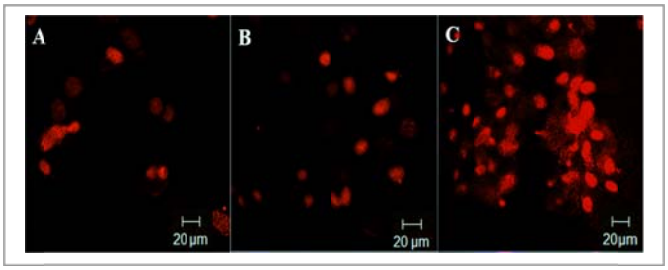

Figure 8. Magic Red TM assay showing the apoptosis-inducing effect (red fluorescence). A) Hyperthermia alone (HEDO-Fe_3O_4, AMF on), B) Chemotherapy alone (HEDO-Fe_3O_4-BTZ), and C) Combined application of hyperthermia and chemotherapy (HEDO-Fe_3O_4-BTZ, AMF on).

Several studies have shown that the efficient eradication of cancer cells are caused by the apoptosis induced cell death mechanism when mild hyperthermia and chemotherapy applied [8, 47, 48]. Therefore we set out to detect the apoptosis inducing ability of the mussel inspired magnetic nanoparticles in hyperthermia alone, chemotherapy alone and the combined scenario using a Magic Red caspase detection kit since caspases 3 and 7, play central roles in triggering apoptotic processes in mammalian cells[49] (Figure 8). Magic Red™ Caspase 3 and 7 Assay Kits measure apoptosis-associated DEVDase enzyme activity in living, intact cells. Hyperthermia alone samples (HEDO-Fe_3O_4, AMF on) and chemotherapy alone samples (HEDO-Fe_3O_4-BTZ, AMF off) displayed a weak red fluorescence (Figure 8A&B) relative to the combined hyperthermia and chemotherapy samples (HEDO-Fe_3O_4-BTZ, AMF on) (Figure 8C). The weak red fluorescence in the hyperthermia alone and chemotherapy alone samples designate that there is a small change in the cellular apoptotic activity due to hyperthermia alone and chemotherapy alone. On the other hand the strong red fluorescence throughout the cytoplasm exhibited by the combined sample indicated that the HEDO-Fe_3O_4-BTZ significantly enhanced the activation of the caspases in the cancer cells through the synergistic effect of both hyperthermia and chemotherapy. This may be due to the enhancement of drug cytotoxicity by the mild hyperthermia application.[47] The results suggest that the thermal improvement of the chemotherapeutic effects along with the concurrent application of hyperthermia significantly induced apoptotic activity in the combined group, resulting in synergistic antitumor effects. Based on the promising results obtained from the *in vitro* studies, we evaluated the potential anticancer efficacy of the bio inspired smart HEDO-Fe_3O_4-BTZ nanoparticles for the *in vivo* (Figure 9). Mice were subcutaneously injected with SCC7 cancer cells ($1x10^6$ cells), and we waited until the tumor size became 100 mm^3. The mice were randomly allocated into three experimental groups of 3 rats each (n=3), namely control, the treated group and the untreated group. The control group was maintained as such without any treatment. The treated (AMF On) and untreated groups (AMF Off) were injected through an intra-tumour route with HEDO-Fe_3O_4-BTZ in PBS solution (40 mg/kg). The enhanced effects of the combined hyperthermia with drug release were determined by treating the one group (treated group) with hyperthermia for 10 minutes on day 1 by placing the mouse in the middle of a water-cooled magnetic induction coil. The AC magnetic fields (293 kHz at 12.57 Oe) were controlled in order to maintain a constant temperature around the tumour, and the same procedures were further repeated two times after three days intervals.

Repeated hyperthermia application was found to have improved the therapeutic efficacy, and thus, after three cycles of hyperthermia therapy, the tumour degradation was evaluated by measuring the weight and volume of the tumour (Figure 9). The samples treated through both hyperthermia and drug delivery exhibited a drastic reduction in the weight and the volume of the tumour relative to both that of the untreated samples and control. The results clearly indicate that the treated samples showed an improvement in the tumour reduction compared to both that of the untreated samples and control; which is in close agreement with the *in vitro* results. The synergistic antitumor effects of HEDO-Fe_3O_4-BTZ treated groups can be attributed due to the improvement in cellular uptake as well as the direct cytotoxicity of repeated application of hyperthermia along with the enhancement of drug cytotoxicity.

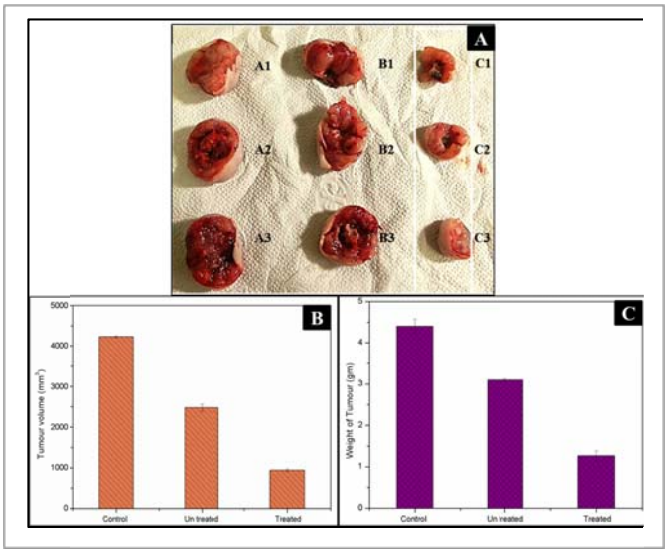

Figure 9. A) Photos of the tumors in mice collected from different groups at the end of the treatments (day 8). (A1-A3) Samples from the control group (n=3), (B1-B3) Samples from the untreated (AMF off) group (n=3), (C1-C3) Samples from the treated (AMF On) group (n=3) , B-C) Average B) volumes and C) weights of tumors collected from different groups of mice at the end of treatments.

4. Conclusions

In conclusion, a smart nanoplatform that is responsive to a magnetic field to administer both hyperthermia and pH-dependent anticancer drug release in a cancer environment has been successfully developed and applied for synergistic anticancer treatment. A mussel-inspired surface functionalization has been carried out using a biocompatible copolymer poly (2-Hydroxyethyl methacrylate-co-dopamine methacrylamide) p(HEMA-co-DMA) accommodating several anchoring groups to produce highly stable HEDO-Fe3O4 nanoparticles. The resulting catechol moieties present in the functionalized SPIONS are exploited for the complexation of anticancer drug BTZ, in a pH-dependent manner to form HEDO-Fe_3O_4-BTZ. The anticancer effect of HEDO-Fe3O4-BTZ on SCC7 cell lines was evaluated and found that the synergistic effect of chemotherapy and hyperthermia enhanced the anticancer effect in SCC7 cells. Thus the HEDO-Fe3O4-BTZ offered the capability to administer as a thermo-chemotherapy agent to improve anticancer effects, even at a very low concentration. Furthermore, HEDO-Fe_3O_4-BTZ showed excellent antitumor efficacy in in vivo cancer treatment study. Thus the BTZ incorporated bio-inspired smart magnetic nanoparticles can act as a safe and effective platform for synergistic anticancer treatment of various types of cancers in the future by acting as both hyperthermic agent that delivers heat when an alternating magnetic field is applied while the BTZ-bound catechol moieties act as chemotherapeutic agents by providing pH-dependent drug release. Even though the present study concentrates on surface tumors, active targeting can be easily employed in the HEDO-Fe_3O_4-BTZ nanoparticles for the synergistic anticancer treatment for deeply existing tumors by further functionalization.

Acknowledgements

This research was supported by grants from the Basic Science Research Program through the National Research Foundation of Korea (NRF), funded by the Ministry of Education, Science and Technology (Project no. 2013-012911 and 2013R1A2A2A04015484).

Notes and references

*Corresponding authors
chskim@jbnu.ac.kr
biochan@jbnu.ac.kr
afeesh@jbnu.ac.kr, afeeshnano@gmail.com

†Electronic Supplementary Information (ESI) availabl (Characterization of p(HEMA-co-DMA) abbreviated as (HEDO) ,XRD spectra of Fe_3O_4 & HEDO-Fe_3O_4, DLS of Fe_3O_4 & HEDO-Fe_3O_4, UV-VIS photospectroscopy of HEDO, BTZ and HEDO-BTZ)

1. Z. Z. J. Lim, J. E. J. Li, C. T. Ng, L. Y. L. Yung and B. H. Bay, *Acta Pharmacologica Sinica*, 2011, **32**, 983-990.
2. Y. Dong, W. K. K. Wu, C. W. Wu, J. J. Y. Sung, J. Yu and S. S. M. Ng, *British Journal of Cancer*, 2011, **104**, 893-898
3. P. B. Santhosh and N. P. Ulrih, *Cancer Letters*, 2013, **336**, 8-17.
4. M. Y. Wu, Q. S. Meng, Y. Chen, P. F. Xu, S. J. Zhang, Y. L. Li, L. X. Zhang, M. Wang, H. L. Yao and J. L. Shi, *Advanced Functional Materials*, 2014, **24**, 4273-4283.
5. P. Guardia, R. Di Corato, L. Lartigue, C. Wilhelm, A. Espinosa, M. Garcia-Hernandez, F. Gazeau, L. Manna and T. Pellegrino, *Acs Nano*, 2012, **6**, 3080-3091.
6. J. Kolosnjaj-Tabi, R. Di Corato, L. Lartigue, I. Marangon, P. Guardia, A. K. A. Silva, N. Luciani, O. Clement, P. Flaud, J. V. Singh, P. Decuzzi, T. Pellegrino, C. Wilhelm and F. Gazeau, *Acs Nano*, 2014, **8**, 4268-4283.
7. K. Hayashi, K. Ono, H. Suzuki, M. Sawada, M. Moriya, W. Sakamoto and T. Yogo, *Chem Mater*, 2010, **22**, 3768-3772.
8. Y. J. Kim, M. Ebara and T. Aoyagi, *Advanced Functional Materials*, 2013, **23**, 5753-5761.
9. J. van der Zee, D. G. Gonzalez, G. C. van Rhoon, J. D. P. van Dijk, W. L. J. van Putten, A. A. M. Hart and D. D. H. Grp, *Lancet*, 2000, **355**, 1119-1125.
10. R. D. Issels, L. H. Lindner, J. Verweij, P. Wust, P. Reichardt, B. C. Schem, S. Abdel-Rahman, S. Daugaard, C. Salat, G. M. Wendtner, Z. Vujaskovic, R. Wessalowski, K. W. Jauch, H. R. Durr, F. Ploner, A. Baur-Melnyk, U. Mansmann, W. Hiddemann, J. Y. Blay, P. Hohenberger, E. O. EORTC-STBSG and ESHO, *Lancet Oncology*, 2010, **11**, 561-570.
11. E. Fantechi, C. Innocenti, M. Zanardelli, M. Fittipaldi, E. Falvo, M. Carbo, V. Shullani, L. D. Mannelli, C. Ghelardini, A. M. Ferretti, A. Ponti, C. Sangregorio and P. Ceci, *Acs Nano*, 2014, **8**, 4705-4719.
12. C. Sanson, O. Diou, J. Thevenot, E. Ibarboure, A. Soum, A. Brulet, S. Miraux, E. Thiaudiere, S. Tan, A. Brisson, V. Dupuis, O. Sandre and S. Lecommandoux, *Acs Nano*, 2011, **5**, 1122-1140.
13. S. X. Huang, K. Shao, Y. Liu, Y. Y. Kuang, J. F. Li, S. An, Y. B. Guo, H. J. Ma and C. Jiang, *Acs Nano*, 2013, **7**, 2860-2871.
14. E. A. Rozhkova, I. Ulasov, B. Lai, N. M. Dimitrijevic, M. S. Lesniak and T. Rajh, *Nano Letters*, 2009, **9**, 3337-3342.

15. B. Sivakumar, R. G. Aswathy, Y. Nagaoka, M. Suzuki, T. Fukuda, Y. Yoshida, T. Maekawa and D. N. Sakthikumar, *Langmuir*, 2013, **29**, 3453-3466.
16. T. Isojima, M. Lattuada, J. B. Vander Sande and T. A. Hatton, *Acs Nano*, 2008, **2**, 1799-1806.
17. D. Pornpattananangkul, S. Olson, S. Aryal, M. Sartor, C. M. Huang, K. Vecchio and L. Zhang, *Acs Nano*, 2010, **4**, 1935-1942.
18. E. Faure, C. Falentin-Daudre, C. Jerome, J. Lyskawa, D. Fournier, P. Woisel and C. Detrembleur, *Prog Polym Sci*, 2013, **38**, 236-270.
19. A. R. U. Amin GhavamiNejad, Arathyram Ramachandra Kurup Sasikala, Melisa Samarikhalaj, Reju George Thomas, Yong Yeon Jeong, Saeed Nasseri, Priya Murugesan, Dongmei Wu, Chan Hee Park, Cheol Sang Kim, *Acs Appl Mater Inter*, 2015, **7**, 12176–12183.
20. A. GhavamiNejad, A. R. K. Sasikala, A. R. Unnithan, R. G. Thomas, Y. Y. Jeong, M. Vatankhah-Varnoosfaderani, F. J. Stadler, C. H. Park and C. S. Kim, *Adv Funct Mater*, 2015, **25**, 2867-2875.
21. S. H. Ku, J. Ryu, S. K. Hong, H. Lee and C. B. Park, *Biomaterials*, 2010, **31**, 2535-2541.
22. S. H. Ku and C. B. Park, *Biomaterials*, 2010, **31**, 9431-9437.
23. J. Jiang, J. Xie, B. Ma, D. E. Bartlett, A. Xu and C. H. Wang, *Acta Biomaterialia*, 2014, **10**, 1324-1332.
24. J. Yu, W. Wei, M. S. Menyo, A. Masic, J. H. Waite and J. N. Israelachvili, *Biomacromolecules*, 2013, **14**, 1072-1077.
25. H. Wei, N. Insin, J. Lee, H. S. Han, J. M. Cordero, W. H. Liu and M. G. Bawendi, *Nano Letters*, 2012, **12**, 22-25.
26. X. S. Liu, J. M. Cao, H. Li, J. Y. Li, Q. Jin, K. F. Ren and J. Ji, *Acs Nano*, 2013, **7**, 9384-9395.
27. Q. Wei, T. Becherer, R. C. Mutihac, P. L. M. Noeske, F. Paulus, R. Haag and I. Grunwald, *Biomacromolecules*, 2014, **15**, 3061-3071.
28. E. Amstad, T. Gillich, I. Bilecka, M. Textor and E. Reimhult, *Nano Letters*, 2009, **9**, 4042-4048.
29. T. Traitel, R. Goldbart and J. Kost, *Journal of Biomaterials Science-Polymer Edition*, 2008, **19**, 755-767.
30. W. H. Chiang, V. T. Ho, W. C. Huang, Y. F. Huang, C. S. Chern and H. C. Chiu, *Langmuir*, 2012, **28**, 15056-15064.
31. J. Liu, Y. R. Huang, A. Kumar, A. Tan, S. B. Jin, A. Mozhi and X. J. Liang, *Biotechnology Advances*, 2014, **32**, 693-710.
32. H. Y. Chen, D. Sulejmanovic, T. Moore, D. C. Colvin, B. Qi, O. T. Mefford, J. C. Gore, F. Alexis, S. J. Hwu and J. N. Anker, *Chem Mater*, 2014, **26**, 2105-2112.
33. J. Min, H. Moon, H. J. Yang, H. H. Shin, S. Y. Hong and S. Kang, *Macromolecular Bioscience*, 2014, **14**, 557-564.
34. J. Su, F. Chen, V. L. Cryns and P. B. Messersmith, *J Am Chem Soc*, 2011, **133**, 11850-11853.
35. S. H. Sun and H. Zeng, *Journal of the American Chemical Society*, 2002, **124**, 8204-8205.
36. M. Vatankhah-Varnoosfaderani, S. Hashmi, A. GhavamiNejad and F. J. Stadler, *Polym Chem-Uk*, 2014, **5**, 512-523.
37. M. Simeonova, G. Ivanova, V. Enchev, N. Markova, M. Kamburov, C. Petkov, A. Devery, R. O'Connor and D. Brougham, *Acta Biomaterialia*, 2009, **5**, 2109-2121.
38. R. Liu, Y. L. Guo, G. Odusote, F. L. Qu and R. D. Priestley, *Acs Appl Mater Inter*, 2013, **5**, 9167-9171.
39. M. Vatankhah-Varnoosfaderani, A. GhavamiNejad, S. Hashmi and F. J. Stadler, *Chem Commun*, 2013, **49**, 4685-4687.
40. P. Drake, H. J. Cho, P. S. Shih, C. H. Kao, K. F. Lee, C. H. Kuo, X. Z. Lin and Y. J. Lin, *Journal of Materials Chemistry*, 2007, **17**, 4914-4918.
41. R. Ghosh, L. Pradhan, Y. P. Devi, S. S. Meena, R. Tewari, A. Kumar, S. Sharma, N. S. Gajbhiye, R. K. Vatsa, B. N. Pandey and R. S. Ningthoujam, *Journal of Materials Chemistry*, 2011, **21**, 13388-13398.
42. G. D. Ayers, E. T. McKinley, P. Zhao, J. M. Fritz, R. E. Metry, B. C. Deal, K. M. Adlerz, R. J. Coffey and H. C. Manning, *J Ultras Med*, 2010, **29**, 891-901.
43. T. Z. Yang, C. M. Shen, Z. Li, H. R. Zhang, C. W. Xiao, S. T. Chen, Z. C. Xu, D. X. Shi, J. Q. Li and H. J. Gao, *J Phys Chem B*, 2005, **109**, 23233-23236.
44. M. S. Wagner, *Anal Chem*, 2005, **77**, 911-922.
45. Q. A. Pankhurst, J. Connolly, S. K. Jones and J. Dobson, *Journal of Physics D-Applied Physics*, 2003, **36**, R167-R181.
46. Y. X. Liu, Z. P. Chen and J. K. Wang, *Journal of Nanoparticle Research*, 2011, **13**, 199-212.
47. A. Hervault and N. T. K. Thanh, *Nanoscale*, 2014, **6**, 11553-11573.
48. N. K. Prasad, K. Rathinasamy, D. Panda and D. Bahadur, *Journal of Materials Chemistry*, 2007, **17**, 5042-5051.
49. W. C. Earnshaw, L. M. Martins and S. H. Kaufmann, *Annual Review of Biochemistry*, 1999, **68**, 383-424.